Biomedicine & Pharmacotherapy 167 (2023) 115443

Contents lists available at ScienceDirect

Biomedicine & Pharmacotherapy

journal homepage: www.elsevier.com/locate/biopha

Treatment of human cardiac fibroblasts with the protein arginine deiminase inhibitor BB-Cl-amidine activates the Nrf2/HO-1 signaling pathway

Aneta Stachowicz [a,b], Alia Sadiq [b], Brian Walker [b], Niveda Sundararaman [c], Justyna Fert-Bober [b,c,*]

[a] Chair of Pharmacology, Jagiellonian University Medical College, Krakow, Poland
[b] Advanced Clinical Biosystems Research Institute, Smidt Heart Institute, Cedars-Sinai Medical Center, Los Angeles, CA, USA
[c] Advanced Clinical Biosystems Research Institute, Precision Biomarker Laboratories, Cedars-Sinai Medical Center, Los Angeles, CA, USA

ARTICLE INFO

Keywords:
Citrullination
Protein arginine deiminase
Proteomics
Cardiac fibrosis
Posttranslational modification
Heme oxygenase 1

ABSTRACT

Background: Cardiac fibrosis contributes to end-stage extracellular matrix remodeling and heart failure (HF). Cardiac fibroblasts (CFs) differentiate into myofibroblasts (myoFbs) to preserve the structural integrity of the heart; however, the molecular mechanisms regulating CF transdifferentiation remain poorly understood. Protein arginine deiminase (PAD), which converts arginine to citrulline, has been shown to play a role in myocardial infarction, fibrosis, and HF. This study aimed to investigate the role of PAD in CF differentiation to myoFbs and identify the citrullinated proteins that were associated with phenotypic changes in CFs.

Results: Gene expression analysis showed that PAD1 and PAD2 isoforms, but not PAD4 isoforms, were abundant in both CFs and myoFbs, and PAD1 was significantly upregulated in myoFbs. The pan-PAD inhibitor BB-Cl-amidine (BB-Cl) downregulated the mRNA expression of PAD1 and PAD2 as well as the protein expression of the fibrosis marker COL1A1 in CFs and myoFbs. Interestingly, a proteomic approach pointed to the activation of the Nrf2/HO-1 signaling pathway upon BB-Cl treatment in CFs and myoFbs. BB-Cl administration resulted in the upregulation of HO-1 at both the gene and protein levels in CFs and myoFbs. Importantly, the protein citrullination landscape of CFs consisting of 86 novel citrullination sites associated with focal adhesion (FN1(R1054)), inflammation (TAGLN(R12)) and DNA replication (EEF2(R767)) pathways was identified.

Conclusions: In summary, we revealed that BB-Cl treatment resulted in increased HO-1 expression via the Nrf2 pathway, which could prevent excessive tissue damage, thereby leading to substantial clinical benefits for the treatment of cardiac fibrosis.

1. Introduction

Heart failure (HF) is a progressive condition that affects a substantial number of people in the U.S. and around the world [1,2]. It is a complex clinical syndrome characterized by the reduced ability of the heart to pump blood [3,4]. The most common conditions leading to HF are coronary artery disease, high blood pressure and previous myocardial infarction (MI) [5]. In response to disease stimuli, cardiac fibroblasts (CFs) differentiate into myofibroblasts (myoFbs), which exhibit proliferative and invasive properties and initiate the reparative healing

Abbreviations: ACEI, angiotensin-converting enzyme inhibitors; ACN, acetonitrile; Act A, activin A; ACTA2, aortic smooth muscle; ARBs, angiotensin receptor blockers; ATP1A1, sodium/potassium-transporting ATPase subunit alpha-1; BB-Cl, BB-Cl-amidine; CFs, cardiac fibroblasts; COL1A1, collagen alpha-1(I) chain; CSE, cystathionine gamma-lyase; CVDs, cardiovascular diseases; DDA, data-dependent acquisition; DIA, data-independent acquisition; ECM, extracellular matrix; EEF2, elongation Factor 2; FASP, filter-aided sample preparation; FC, fold change; FDR, false discovery rate; FN1, fibronectin 1; GCLC, glutamate-cysteine ligase catalytic subunit; HF, heart failure; HO-1/2, heme oxygenase-1/-2; IL, interleukin; IPA, ingenuity pathway analysis; LC—MS/MS, liquid chromatography – tandem mass spectrometry; LOXL2, lysyl oxidase homolog 2; myoFbs, myofibroblasts; Nrf2, nuclear factor erythroid 2-related factor 2; PAD, protein arginine deiminase; PINE, protein interaction network extractor; PTM, posttranslational modification; RBM24, RNA-binding protein 24; RT—qPCR, quantitative reverse transcription polymerase chain reaction; SM22α, smooth muscle 22α; SOD2, superoxide dismutase [Mn], mitochondrial; SREBP, sterol regulatory element binding protein; SULF1, extracellular sulfatase Sulf-1; SULT1A1, sulfotransferase 1A1; TAGLN, transgelin; TGF-β1, transforming growth factor beta-1; TLN1, talin-1.

* Correspondence to: Advanced Clinical Biosystems Research Institute, Smidt Heart Institute, Cedars-Sinai Medical Center, 127 S San Vicente Blvd, Los Angeles, CA 90048, USA.

E-mail address: Justyna.Fert-Bober@cshs.org (J. Fert-Bober).

https://doi.org/10.1016/j.biopha.2023.115443
Received 26 May 2023; Received in revised form 27 August 2023; Accepted 4 September 2023
Available online 11 September 2023

response [6]. Importantly, the activation of CFs into myoFbs is a critical step in the development of cardiac fibrosis [7].

Extensive research in the last decade has revealed that post-translational modifications (PTMs), including phosphorylation, ubiquitination, methylation, acetylation, SUMOylation, and succinylation, play important roles in pathological cardiac hypertrophy pathways [8]. In recent years, citrullination, an irreversible enzymatic PTM in which arginine is converted to citrulline, an atypical residue, has gained increasing attention due to its involvement in various physiologic and pathologic conditions [9]. The loss of a positive charge on the arginine residue due to citrullination perturbs the number of intra- and intermolecular electrostatic interactions, causing alterations in protein structure and function. The protein arginine deiminase (PAD) family of enzymes, PAD1, PAD2, PAD3, PAD4 and PAD6, which share 50–90% sequence identity, catalyzes citrullination in the presence of excess calcium [10]. PAD dysregulation and increased citrullination have been associated with epigenetic events [11], pluripotency [12], immunity [13], and transcriptional regulation [14]. Current research often investigates citrullination, neutrophil trap (NET) formation, PAD overexpression, and extracellular DNA accumulation in chronic diseases, such as rheumatoid arthritis [15], multiple sclerosis [16] and age-related organ fibrosis dysfunctions [17–19]. The ability of PAD4-mediated histone citrullination to induce NETosis in an aged fibrotic mouse model [18,19] prompted us to ask whether PAD can play a role in the fibrosis process through processes other than NETosis.

In this study, we investigated the role of PADs in the differentiation of CFs to myoFbs and elucidated the mechanisms involved. We determined the citrullinated proteins and modified arginines that are associated with this biological switch using state-of-the-art proteomics methods. We hope that revealing the comprehensive citrullinated proteome and its rearrangement following the activation of CFs could lead to important clinical benefits for the treatment of cardiac fibrosis.

2. Methods

2.1. Human cardiac fibroblast (CF) cell culture

Human cardiac fibroblast (CF) primary cells (source: normal human fetal heart from a single donor: Caucasian 21 weeks gestation) were obtained from Sigma Aldrich (St. Louis, MO, USA; catalog number: 306–05 F) and grown in a humidified incubator containing 5% CO_2 and 95% air at 37 °C in DMEM/F12 medium (Gibco, Waltham, MA, USA) supplemented with 10% fetal bovine serum (FBS, Gibco, Waltham, MA, USA) and 1% antibiotic-antimycotic 100X (Gibco, Waltham, MA, USA). CFs were cultured on dishes coated with 0.2% gelatin and subcultured every 2–3 days using TripLE Express enzyme (Gibco, Waltham, MA, USA) until passage number 7. One day before stimulation, the cells were starved in 1% FBS and then activated with 10 ng/ml TGF-β1 (R&D Systems, Minneapolis, MN, USA) for 24 h to initiate myoFb differentiation. The pan-PAD inhibitor BB-Cl-amidine (500 nM) was added 15 min before stimulation with TGF-β1. The toxicity of BB-Cl-amidine was evaluated at 24 h using MTT assays.

2.2. MTT metabolism assay

To assess CF cell viability after 24 h of BB-Cl-amidine treatment, 10 μL of a 10 mg/ml MTT solution (Sigma—Aldrich, St. Louis, MO, USA) was added to each well and incubated at 37 °C for 1 h. Then, the medium was aspirated, 200 μL of DMSO was added, and the plate was shaken for 1 h to dissolve the dye. The absorbance was measured at 570 nm using a Synergy™ 2 microplate reader (BioTek Instruments Inc., Winooski, VT, USA).

2.3. Quantitative reverse transcription polymerase chain reaction (RT–qPCR)

The expression levels of genes related to the differentiation of cardiac fibroblasts to myofibroblasts (*COL1A1, ACTA2, TGF-B1, FN-1, LOXL2, IL-6, HO-1*) and PAD isoforms (*PAD1, PAD2, PAD3, PAD4*) were determined according to a previously described protocol [20]. Briefly, RNA was isolated using the ReliaPrep™ RNA Cell Miniprep System (Promega, Madison, WI, USA) and transcribed to cDNA with the High-Capacity cDNA Reverse Transcription Kit (Thermo Scientific, Waltham, MA, USA). The primers used in these experiments included *COL1A1*: 5′ GGACACAGAGGTTTCAGTGGT 3′ (forward), 5′ CAC CATCATTTCCACGAGCA 3′ (reverse); *ACTA2*: 5′ ACTGCCTTGGTGTGTGACAATGG 3′ (forward), 5′ TGGTGCCAGATCTTTTCCATG 3′ (reverse); *TGF-B1*: 5′ GCAGCACGTGGAGCTGTA 3′ (forward), 5′ CAGCCGGTTGCTGAGGTA 3′ (reverse); *FN-1*: 5′ AGCAGACCCAGCTTAGAGTT 3′ (forward), 5′ GCAGAAGTGTTTGGGTGACT 3′ (reverse); *LOXL2*: 5′ GCGTCACTGACTGCAAGCAC 3′ (forward), 5′ CGAATCCGA ATGTCCTCCAC 3′ (reverse); *IL6*: 5′ ACTCACCTCTTCAGAACGAATTG 3′ (forward), 5′ CCATCTTTGGGAGGTTCAGGTTG 3′ (reverse); *PAD3*: 5′ CTGGATTGCGACCTGAACTG 3′ (forward), 5′ TGTGGTCATCAAAGAGGGCT 3′ (reverse); *PAD4*: 5′ ACTCTCCAAGGAACAGAGG 3′ (forward), 5′ GGTATTCCTTGCCCCTGACT 3′ (reverse) and 2x SsoAdvanced™ Universal SYBR® Green Supermix (Bio-Rad, Hercules, CA, USA) was used for real-time PCR. Primers for *PAD1*, *PAD2*, *GAPDH* and *HO-1* were commercially ordered from Bio-Rad (Hercules, CA, USA) and RealTimePrimers (Mountain Ave, PA, USA). Analysis of relative gene expression was performed by the CFX96 Touch Real-Time PCR Detection System (Bio-Rad, Hercules, CA, USA) with *GAPDH* as an internal reference gene, and the data were analyzed using the $2^{-\Delta\Delta Ct}$ method in an Excel spreadsheet.

2.4. Immunoprecipitation (IP)

Fifty microliters of Dynabeads Protein G coupled magnetic beads (Invitrogen, Waltham, MA, USA) was washed with PBS and then incubated with 2.5 μg of the corresponding antibodies anti-PAD1 (Cayman, Ann Arbor, MI, USA), anti-PAD2 (Abcam, Cambridge, UK) and anti-PAD4 (Abcam, Cambridge, UK) at room temperature for 1 h. Then, the protein lysate samples (50 μg) were incubated with antibodies bound to magnetic beads for 16–20 h at 4 °C. The next day, the reaction solution was washed two times with 50 mM Tris/10 mM NaCl, pH 8.5. After thorough washing, the purified proteins were eluted with 1 × Laemmli sample buffer (Sigma). IP samples (20 μL) were separated by SDS—PAGE and then transferred onto PVDF membranes using the Trans-Blot Turbo Transfer System (Bio-Rad, Hercules, CA, USA) as described below to confirm the presence of PADs. As a positive control, a PAD cocktail (active) (SignalChem, British Columbia, Canada) was used.

2.5. Western blot

CFs were lysed in 2% SDS and 50 mM DTT in 0.1 M Tris-HCl (pH 7.6). The protein concentration was measured by a Pierce 660 nm Protein Assay Kit (Thermo Scientific, Waltham, MA, USA). Cell lysates containing equal amounts of total protein were mixed with 4x Laemmli Sample Buffer (Bio-Rad, Hercules, CA, USA) and incubated at 96 °C for 5 min. Protein samples (10 μg of protein per well) were separated on SDS-polyacrylamide gels (4–15%) (Criterion™ TGX™ Precast Gels, Bio-Rad, Hercules, CA, USA) using a Laemmli buffer system and then semidry transferred to PVDF membranes by a Trans-Blot Turbo Transfer System (Bio-Rad, Hercules, CA, USA). The membranes were blocked with 5% bovine serum albumin in PBS at room temperature for 1 h and incubated overnight at 4 °C with specific anti-collagen I (Abcam, Cambridge, UK) and anti-HO-1 (Proteintech, Rosemont, IL, USA) (concentration 1:1000) as well as anti-PAD1 (Cayman, Ann Arbor, MI, USA), anti-PAD2 (Abcam, Cambridge, UK) and anti-PAD4 (Abcam,

Cambridge, UK) (concentration 1:500) primary antibodies. Incubation with HRP-conjugated secondary antibodies (Bio-Rad, Hercules, CA, USA) was performed at room temperature for 1 h (dilution 1:10 000). Protein bands were developed by applying Clarity™ Western ECL Substrate (Bio-Rad, Hercules, CA, USA) for 1 min. Precision Plus Protein Kaleidoscope Standards (Bio-Rad, Hercules, CA, USA) were used for molecular weight determinations. Protein bands were visualized and imaged by using an ImageQuant LAS 4000 scanner (GE Healthcare, Chicago, IL). Later, the blot was stained with Direct Blue 71 (Sigma—Aldrich, St. Louis, MO, USA) and developed for total protein level normalization.

2.6. Liquid chromatography-tandem mass spectrometry (LC—MS/MS) analysis of CFs

CFs were lysed in a buffer containing 0.1 M Tris-HCl, pH 7.6, 2% SDS, and 50 mM DTT (Sigma Aldrich, St. Louis, MO, USA) at 96 °C for 10 min. The protein concentration was determined by a Pierce 660 nm Protein Assay Kit (Thermo Scientific, Waltham, MA, USA). Seventy micrograms of protein was digested overnight using the filter-aided sample preparation (FASP) method [21,22] with endoproteinase Lys-C (enzyme-to--protein ratio 1:35) as the digestion enzyme [23]. Next, the samples were cleaned on an Oasis HLB plate (Waters, Milford, MA, USA) prior to LC−MS/MS analysis. All samples were dissolved in 0.1% formic acid at a concentration of 0.5 μg/μL and spiked with the iRT peptides (Biognosys, Schlieren, Switzerland).

One microgram of peptide was analyzed by LC–MS/MS using an Ultimate 3000 LC and an Orbitrap Lumos Fusion MS (Thermo Fisher Scientific, Waltham, MA, USA). An M3 multinozzle emitter (Newomics, Berkeley CA, USA) was used to electrospray eluting peptides into the mass spectrometer at 3.9 kV with the sheath gas set to 20 (arbitrary units). Peptides were loaded into a Luna Omega trapping column (300 μm I.D. × 2 cm, Polar C18 3 μm, 100 Å, Phenomenex) and separated over a 60-minute reversed-phase gradient at 8 μL/min on a Luna Omega analytical column (300 μm I.D. × 15 cm, Polar C18 3.0 μm, 100 Å). The analytical gradient started at 5% mobile phase B (0.1% formic acid in acetonitrile). The mobile phase B composition linearly increased to 30% at 45 min, then increased to 40% at 50 min, and finally linearly increased to 45% B at 60 min. Mass spectrometry data were acquired using a data-independent method (DIA) and a data-dependent method (DDA) for library preparation. The precursor MS1 scans were acquired at 120 K resolution and spanned the 400–1000 m/z range. The maximum injection time was set to 50 ms, and the AGC target was set to 400,000. After each MS1 scan, the entire 400–1000 m/z range was fragmented by HCD with 30% normalized energy in nonoverlapping 15 m/z windows (40 DIA scans following each MS1 scan). The DIA scans were acquired at 15 K resolution with AGC set to 500,000 and a maximum injection time of 30 ms.

DDA data were searched against the human UniProt database and MaxQuant Contaminants list using the Pulsar search engine in Spectronaut software (Biognosys, Schlieren, Switzerland)[24] with the following parameters: ± 40 ppm mass tolerance on MS1 and MS2 level, mutated decoy generation method, Lys-C enzyme specificity, 1% protein and PSM false discovery rate (FDR). The library was generated using 3–6 fragment ions per precursor. The generated CF library was used to analyze DIA data in Spectronaut software. Data were filtered by 1% FDR at the peptide and protein levels, while quantitation and interference correction were performed at the MS2 level. The data were normalized by a global regression strategy, and Q-value filtering without imputation was applied. Statistical analysis of differential protein abundance was performed at both MS1 and MS2 levels [25] using unpaired t tests with multiple testing correction after Story [26].

2.7. Mapping citrullination sites using a hypercitrullinated library approach

To prepare a hypercitrullinated library, CFs were lysed as previously described. To digest proteins and preserve citrullinated residues, the FASP method with Lys-C as the digestion enzyme was used. The deimidation reaction was performed using Microcon-30 centrifugal filters during the FASP protocol as previously described [23]. Then, the samples were desalted on an Oasis HLB plate (Waters, Milford, MA, USA). To prepare the library, samples were fractionated using a Pierce™ High pH Reversed-Phase Peptide Fractionation Kit (Thermo Fisher Scientific, Waltham, MA, USA) according to the manufacturer's instructions with the modification that each sample was fractionated into 5 fractions with 7.5%, 10%, 12.5%, 15% and 17.5% ACN in elution solution. Next, the samples were run on LC—MS/MS in DDA mode as previously described [27]. A hypercitrullinated library was prepared using SpectraST v.4.0. Briefly, all data were searched using X! Tandem Native v.2013.06.15.1, X! Tandem Kscore v.2013.06.15.1, and Comet v.2014.02 rev.2. The search parameters included the following criteria: static modifications of carbamidomethyl (C) and variable modifications of oxidation (M), deamidation (NQ), and citrullination (R). The parent mass tolerance was set at 50 ppm, and the monoisotopic fragment mass tolerance was 100 ppm (which was further filtered to be <0.05 Da to build the spectral library); LysC peptides with up to two missed cleavages were allowed. The identified peptides were processed and analyzed by Trans-Proteomic Pipeline v.4.8 and were validated using PeptideProphet scoring, and the PeptideProphet results were statistically refined using iProphet. All peptides were filtered at an FDR of 1% with a peptide probability cutoff of ≥ 0.99. To identify citrullinated peptides from DIA runs, a hypercitrullinated spectral library generated by SpectraST was used with CitFinder software to analyze modified-unmodified peptide pairs for physicochemical properties such as ΔRT shift, charge state and neutral loss [27]. Statistical analysis of citrullinated peptides was performed in Perseus [28]. Citrullinated peptide quantities were normalized to their corresponding protein levels. ANOVA with post hoc tests and permutation-based FDR correction were used for the statistical analysis of data in Perseus.

2.8. Constructing protein–protein interaction (PPI) networks

Functional grouping and pathway analysis were performed using PINE (Protein Interaction Network Extractor) software [29] with the STRING and GeneMANIA databases using a score confidence of 0.4 and a ClueGO p value cutoff < 0.05. The mass spectrometry data have been deposited to the ProteomeXchange Consortium via the PRIDE partner repository [30] with the dataset identifier PXD040885.

2.9. Ingenuity pathway analysis (IPA)

Datasets from LC—MS/MS experiments representing differentially expressed proteins were imported into Ingenuity Pathway Analysis (IPA, Winter Release 2022; Ingenuity Systems, Redwood City, CA, USA; http://www.ingenuity.com) to determine upstream regulators. Upstream regulators are a set of proteins/molecules that regulate the expression of downstream molecules in a biological network. IPA was also used to identify the functional pathways and biological networks. In the network, molecules are represented as nodes, and relationships between two nodes are represented as lines. All lines were supported by at least 1 reference from the literature, a textbook, or canonical information stored in the Ingenuity Pathway Knowledge Base. Nodes were displayed using various shapes that represent the functional class of the protein.

2.10. Statistical analysis

Data are expressed as the mean ± SEM. The equality of variance and normality of the data were checked by the Brown-Forsythe test and

Shapiro—Wilk test, respectively. Based on the results, statistical analysis was performed using classic one-way ANOVA, Brown-Forsythe and Welch ANOVA or Kruskal—Wallis tests with correction for multiple comparisons by controlling the false discovery rate (two-stage linear step-up procedure of Benjamini, Krieger and Yekutieli) (GraphPad Prism 9.3.1, San Diego, CA, USA). Values of $p < 0.05$ (or q-values for proteomics experiments) were considered statistically significant.

3. Results

3.1. PAD1 and PAD2 are the most abundant PAD isoforms in CFs

We postulated that CFs express PAD isoforms and that TGF-β1 alters their expression as a part of fibrosis pathogenesis. We first investigated the PAD1, PAD2, PAD3 and PAD4 mRNA expression levels in CFs using quantitative RT—PCR. The most abundant PAD isoforms in untreated CFs (control) were PAD1 (cycle threshold (Ct) = 29.8 ± 0.1) and PAD2 (Ct = 32.3 ± 0.1), followed by PAD4 (Ct = 35.1 ± 0.2). We did not detect any mRNA expression of PAD3. To activate CFs, we treated CFs with 10 ng/ml TGF-β1 for 24 h to induce their differentiation into myoFbs. This differentiation resulted in upregulated mRNA expression of fibrosis markers, including collagen alpha-1(I) chain (COL1A1) (FC = 1.52 ± 0.10 vs. FC = 1.02 ± 0.10 in control, $p < 0.05$), actin, aortic smooth muscle (ACTA2) (FC = 1.53 ± 0.03 vs. FC = 1.03 ± 0.10 in control, $p < 0.05$), transforming growth factor beta-1 (TGF-B1) (FC = 1.29 ± 0.05 vs. FC = 1.01 ± 0.06 in control, $p < 0.05$), and interleukin 6 (IL-6) (FC = 1.83 ± 0.08 vs. FC = 1.04 ± 0.11 in control, $p < 0.001$), in TGF-β1-stimulated CFs (Fig. 1D, E, F and G). Similarly, we observed a statistically significant increase in PAD1 mRNA expression levels (FC = 1.41 ± 0.15 vs. FC = 1.02 ± 0.08 in control, $p < 0.01$) in CFs treated with TGF-β1 compared to control CFs. PAD2 expression only marginally increased (Fig. 1B) compared to PAD4 expression, which did not considerably change or even declined compared to control CFs (Fig. 1C).

To test whether inhibition of PAD affects fibrosis, CFs were stimulated with TGF-β1 in the presence of the pan-PAD inhibitor BB-Cl-amidine. In our experiments, we chose a dose of BB-Cl-amidine equal to 500 nM based on the results of the MTT cell viability assay (Fig. 1H). The stimulation with TGF-β1 in the presence of BB-Cl did not influence cell viability (see Supplemental Fig. 1). Importantly, BB-Cl treatment led to the downregulation of both PAD1 (FC = 0.62 ± 0.04 in BB-Cl group vs. FC = 1.02 ± 0.08 in control, $p < 0.001$; FC = 0.77 ± 0.09 in TGF-β1 + BB-Cl group vs. FC = 1.41 ± 0.15 in TGF-β1 group, $p < 0.0001$) and PAD2 (FC = 0.54 ± 0.04 in BB-Cl group vs. 1.02 ± 0.08 in control, $p < 0.001$; FC = 0.55 ± 0.04 in TGF-β1 + BB-Cl group vs. FC = 1.10 ± 0.13 in TGF-β1 group, $p < 0.0001$) mRNA expression in control cells and myoFbs (Fig. 1A and B). Conversely, BB-Cl-amidine treatment upregulated the mRNA expression of PAD4 (FC = 1.47 ± 0.28 in the TGF-β1 + BB-Cl group vs. FC = 0.89 ± 0.08 in the TGF-β1 group, $p < 0.05$) (Fig. 1C). This result might reflect the compensatory role of PAD4 in CFs stimulated with TGF-β1 upon pharmacological inhibition of PADs.

By western blot analysis, a 74 kDa band for PADs was detected in IP extracts of the in vitro cell culture model, confirming the presence of PADs in CFs (see Supplemental Fig. 2). Immunosignal densities were detected for PAD1 and PAD2 at the protein level, with a higher signal for PAD1 in control samples. The immunosignal for PAD2 was very faint, possibly due to the proximity of the 75 kDa IgG band that had been eluted from beads. Meanwhile, we did not detect PAD4 at the protein

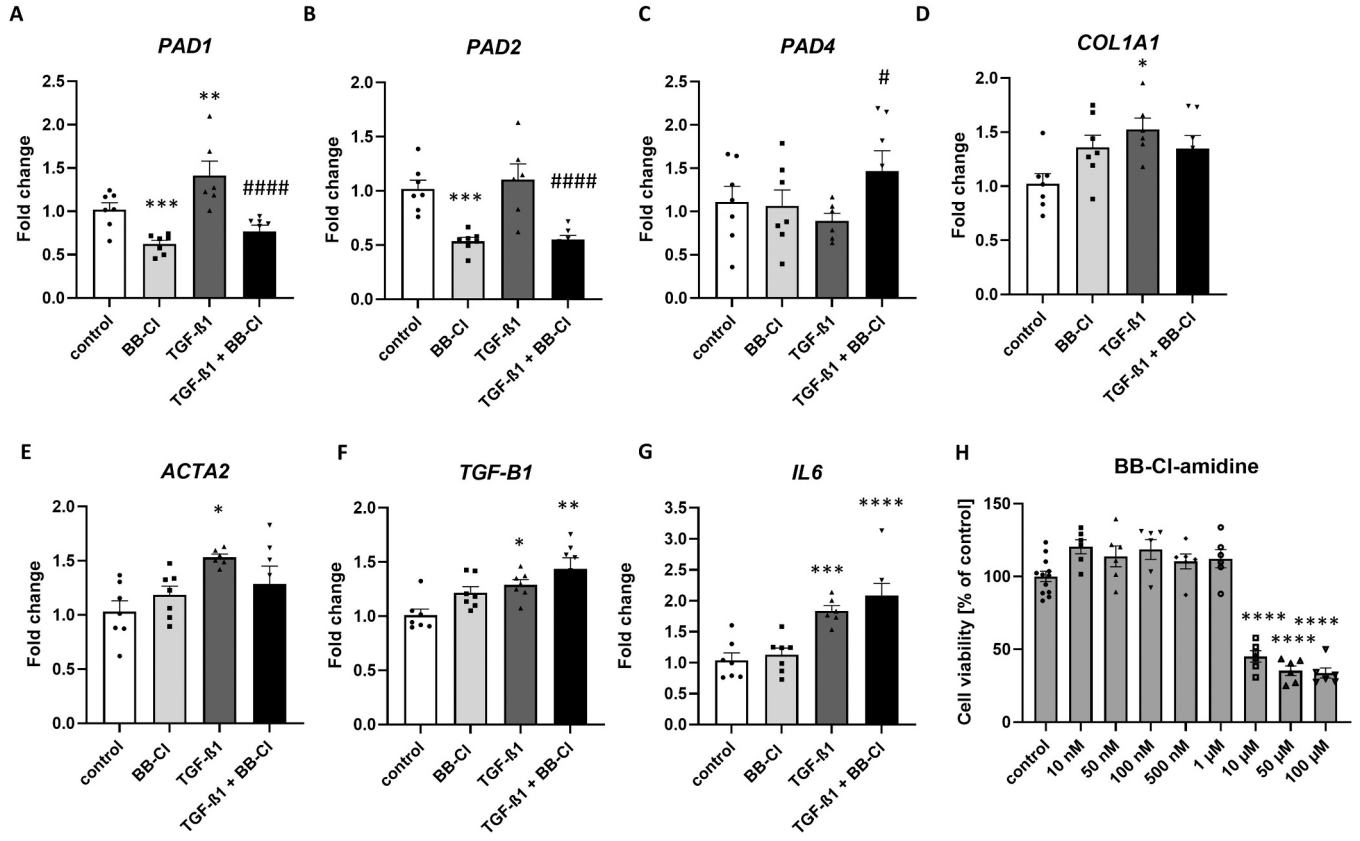

Fig. 1. PAD expression in CFs stimulated with TGF-β1 to myoFbs. PAD1 was upregulated in TGF-β1-stimulated CFs and downregulated in response to treatment with the pan-PAD inhibitor BB-Cl-amidine. mRNA expression of PAD1 A), PAD2 B), and PAD4 C) in TGF-β1-stimulated CFs for 24 h in the presence of BB-Cl. mRNA expression of the fibrosis markers COL1A1 D), ACTA2 E), TGF-β1 F), and IL-6 G) in CFs treated with TGF-β1 for 24 h in the presence of BB-Cl. The toxicity of BB-Cl-amidine in CFs was measured using MTT assays at 24 h H). Mean ± SEM; *$p < 0.05$, **$p < 0.01$, ***$p < 0.001$, ****$p < 0.0001$ compared to control; #$p < 0.05$, ####$p < 0.0001$ compared to TGF-β1; $n = 7$.

level, which suggests that the low amount of PAD4 mRNA present in CFs was not translated to protein (Supplemental Fig. 2).

3.2. Proteomic analysis reveals pathways associated with BB-Cl administration, including the Nrf2-mediated oxidative stress response pathway

To comprehensively investigate the changes in protein expression and citrullination profiles that occur during CF differentiation into myoFbs, a qualitative proteomics analysis was conducted. LC—MS/MS measurements operated in DDA mode identified 27,822 proteotypic peptides, providing a human cardiac fibroblast spectral library composed of 5163 protein groups. The obtained library was used to analyze DIA runs in Spectronaut. Spectral library recovery was 72.7%, and the median protein group CV was approximately 15% (Supplemental Fig. 3), which allowed for the calculation of a significant cutoff equal to a fold change of 1.25 (statistical power greater than 80%). A summary of the quality control for the LC—MS/MS runs is shown in Supplemental Fig. 3. In summary, 3554 protein groups across all biological conditions were identified and quantified. Using cutoffs of $q < 0.05$ and $\log2FC \leq 0.322$, we found a total of 171 proteins altered in BB-Cl-amidine–treated CFs compared to control cells and 187 proteins altered in TGF-β1-stimulated cells compared to control cells. Furthermore, we identified 181 differentially expressed proteins upon BB-Cl-amidine treatment in TGF-β1-stimulated CFs in comparison to TGF-β1-stimulated cells (Fig. 2A, B and C). Among several proteins potentially involved in the beneficial mechanisms of BB-Cl treatment in CFs differentiated into myoFbs, cystathionine gamma-lyase (CSE) was upregulated (FC = 1.39) upon BB-Cl administration in TGF-β1-stimulated cells. In contrast, extracellular sulfatase Sulf-1 (SULF1), activin A (Act A) and RNA-binding protein 24 (RBM24) were all downregulated (FC = −1.61; FC = −1.47 and FC = −1.75, respectively, in comparison to the TGF-β1 group) in CFs activated to myoFbs upon BB-Cl-amidine treatment (Supplemental Table 1). The detailed list of differentially expressed proteins and their fold changes across all biological conditions are presented in Supplemental Table 1.

To identify the functional pathways and biological networks as well as upstream regulators, we performed enriched pathway analysis based on protein expression (PINE) and gene expression (IPA). Enriched functional networks generated by PINE indicated that the metabolism of the amino acid pathway was activated, shown as orange central nodes, and VEGF signaling, cholesterol biosynthesis, and sterol regulatory element binding protein (SREBP) pathways were inhibited, shown as blue central nodes (Fig. 2D). In turn, IPA analysis pointed to altered integrin and actin cytoskeleton signaling in CFs differentiated into myoFbs and treated with BB-Cl-amidine (Table 1). Detailed network analyses by IPA in CFs treated with TGF-β1 and BB-Cl-amidine are shown in Supplemental Fig. 4. In addition, using IPA, we identified upstream regulators in CFs related to TGF-β1 stimulation and BB-Cl-amidine treatment (Table 2). Based on the network analysis, nuclear factor erythroid 2-related Factor 2 (NFE2L2 or Nrf2), which has been described as a master transcription factor responsible for the activation of antioxidant genes in response to oxidative stress, was identified as an upstream regulator in CFs upon BB-Cl-amidine administration (Table 2).

3.3. BB-Cl administration upregulates expression of heme oxygenase-1 (HO-1)

Our proteomic analysis identified upregulated expression of heme oxygenase-1 (HO-1) in CFs activated to myoFbs in the presence of BB-Cl-

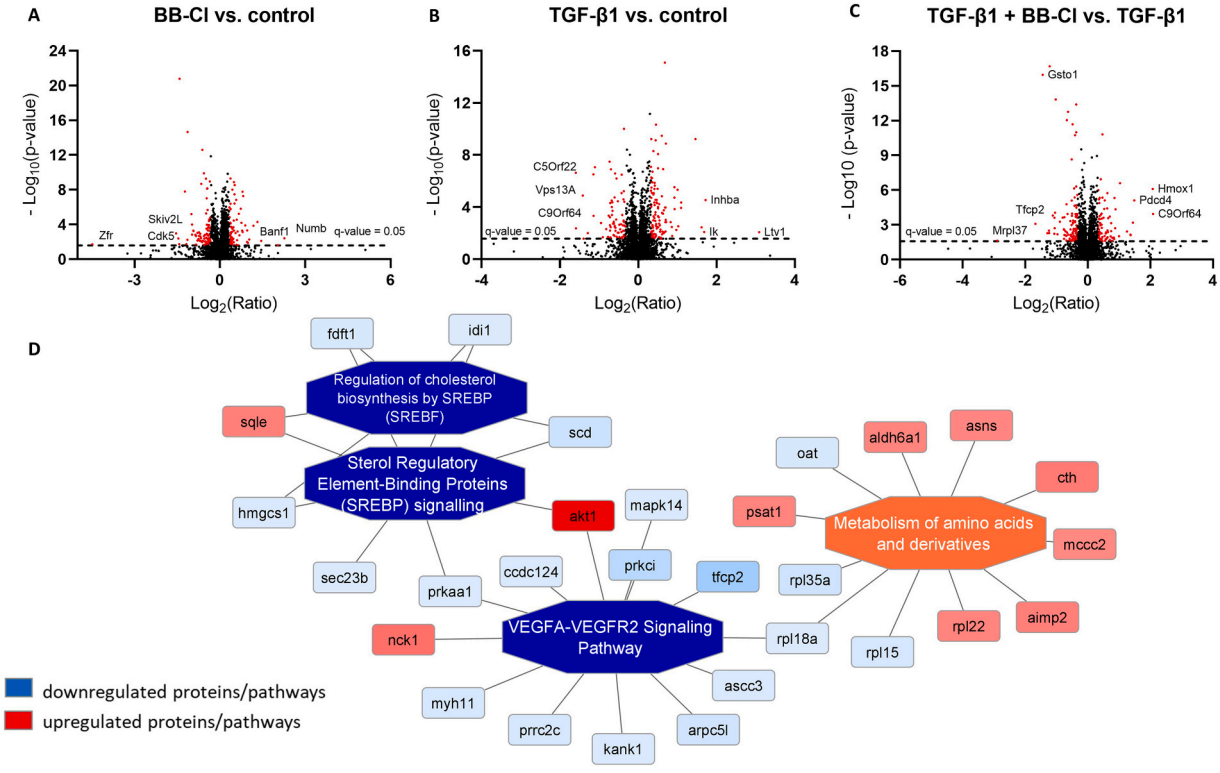

Fig. 2. Proteomics results and functional network analysis of CFs stimulated with TGF-β1 in the presence of the pan-PAD inhibitor BB-Cl-amidine. BB-Cl administration downregulated pathways related to cholesterol biosynthesis and VEGF signaling. Volcano plot of differentially expressed proteins showing the log2 ratio of protein expression versus -log10 p value. A) BB-Cl-treated CFs compared to control, B) TGF-β1-stimulated CFs compared to control and C) TGF-β1-stimulated CFs treated with BB-Cl compared to TGF- β1-stimulated cells. The most upregulated and downregulated proteins are shown. D) Enriched functional network in TGF-β1-stimulated CFs treated with BB-Cl compared to TGF-β1-stimulated cells, as generated by PINE. Activated pathways are shown as orange central nodes, and inhibited pathways are shown as blue central nodes along with red (upregulated) or blue (downregulated) protein nodes. q-value < 0.05; n = 6–7.

Table 1
Top five canonical pathways identified by IPA in CFs treated with TGF-β1 and BB-Cl-amidine (n = 6–7).

	Top Canonical Pathways	p value	Overlap
BB-Cl-amidine vs. control			
1	Integrin Signaling	1.05E-26	31.0%
2	BAG2 Signaling Pathway	8.12E-25	47.6%
3	Protein Ubiquitination Pathway	4.65E-24	26.2%
4	FAT10 Signaling Pathway	2.38E-23	57.1%
5	Inhibition of ARE-Mediated mRNA Degradation Pathway	2.04E-21	31.7%
TGF-β1 vs. control			
1	EIF2 Signaling	8.34E-53	43.9%
2	Regulation of eIF4 and p70S6K Signaling	2.32E-32	38.2%
3	Protein Ubiquitination Pathway	1.20E-22	26.2%
4	mTOR Signaling	8.90E-22	28.9%
5	Actin Cytoskeleton Signaling	1.52E-19	25.7%
TGF-β1 + BB-Cl-amidine vs. TGF-β1			
1	Protein Ubiquitination Pathway	1.99E-18	22.5%
2	Integrin Signaling	6.29E-18	24.9%
3	NRF2-mediated Oxidative Stress Response	7.59E-18	23.7%
4	Actin Cytoskeleton Signaling	2.06E-16	22.4%
5	Caveolar-mediated Endocytosis Signaling	4.92E-14	36.0%

amidine (FC = 4.22 in comparison to the TGF-β1 group) but not heme oxygenase-2 (HO-2) (Supplemental Table 1; Fig. 3F and G). We also confirmed upregulated expression of HO-1 in the BB-Cl group as well as the TGF-β1 + BB-Cl group using RT—qPCR (FC = 7.89 ± 0.78 in BB-Cl group vs. 1.06 ± 0.15 in control, $p < 0.0001$; FC = 4.76 ± 1.00 in TGF-β1 + BB-Cl group vs. FC = 0.79 ± 0.13 in TGF-β1 group, $p < 0.0001$) (Fig. 3E). Western blot experiments validated the results of upregulated HO-1 expression in CFs upon BB-Cl treatment (3.29 ± 0.24 in the BB-Cl group vs. 0.96 ± 0.15 in the control, $p < 0.001$; 3.18 ± 0.55 in the TGF-β1 + BB-Cl group vs. 0.91 ± 0.08 in the TGF-β1 group, $p < 0.001$) (Fig. 3A and B; Supplemental Fig. 5). The effect of upregulated expression of HO-1 was associated with the downregulated expression of the fibrosis marker COL1A1 in TGF-β1-stimulated CFs upon treatment with BB-Cl-amidine (FC = −1.32 in comparison to the TGF-β1 group) (Supplemental Table 1; Fig. 3H). A similar trend of downregulated COL1A1 protein expression after BB-Cl administration was confirmed by Western blotting (Fig. 3A and C) in CFs and CFs activated to myoFbs. Moreover, we found that the 35 kDa COL1A1 C-terminal propeptide was upregulated upon BB-Cl treatment in CFs and TGF-β1-stimulated CFs (0.15 ± 0.02 in BB-Cl group vs. 0.05 ± 0.02 in control, $p < 0.01$; 0.15 ± 0.02 in TGF-β1 + BB-Cl group vs. 0.06 ± 0.02 in TGF-β1 group, $p < 0.01$) (Fig. 3A and D; Supplemental Fig. 5). This may indicate that treatment with BB-Cl increased COL1A1 degradation in CFs and myoFbs. Importantly, other cytoprotective proteins, including sulfotransferase 1A1 (SULT1A1), superoxide dismutase [Mn], mitochondrial (SOD2) and glutamate-cysteine ligase (GCLC) (FC = 4.81, FC = 1.54 and FC =1.31, respectively), were upregulated in BB-Cl-treated cells (Supplemental Table 1). All these proteins have been reported to be regulated by the transcription factor Nrf2.

Table 2
Top five upstream regulators identified by IPA in CFs treated with TGF-β1 and BB-Cl-amidine (n = 6–7).

	Top Upstream Regulators	Name	p value	Predicted Activation
BB-Cl-amidine vs. control				
1	TP53	Tumor protein p53	3.22E-54	Activated
2	MYC	Myc proto-oncogene protein	2.32E-41	Activated
3	MAPT	Microtubule associated protein tau	1.85E-31	Activated
4	NFE2L2	Nuclear factor erythroid 2-related Factor 2	8.15E-30	Activated
5	XBP1	X-box-binding protein 1	2.37E-24	Activated
TGF-β1 vs. control				
1	LARP1	La-related protein 1	5.17E-50	Inhibited
2	MYC	Myc proto-oncogene protein	2.88E-48	Activated
3	LH	Luteinizing hormone	5.82E-45	Activated
4	TP53	Tumor protein p53	3.60E-40	Activated
5	MLXIPL	Carbohydrate-responsive element-binding protein	4.25E-33	Activated
TGF-β1 + BB-Cl-amidine vs. TGF-β1				
1	TP53	Tumor protein p53	3.65E-49	Activated
2	CLPP	ATP-dependent Clp protease proteolytic subunit, mitochondrial	7.13E-35	Inhibited
3	MYC	Myc proto-oncogene protein	2.58E-34	Activated
4	NFE2L2	Nuclear factor erythroid 2-related Factor 2	2.58E-23	Activated
5	MMP12	Macrophage metalloelastase	2.69E-23	Activated

3.4. The protein citrullination landscape of human cardiac fibroblasts consists of many structural proteins

Next, we sought to identify the citrullinated targets of PADs in human CFs. Using MS analysis based on a hypercitrullinated library, we quantified 86 citrullinated sites, 85 citrullinated peptides and 68 citrullinated proteins in CFs (Supplemental Table 2). In our study, quantified citrullinated proteins were engaged, among others, in neutrophil degranulation, focal adhesion, DNA processing, translation elongation, proteasomal degradation, cellular response to stress, IL-4 and IL-13 signaling, protein processing in the endoplasmic reticulum and VEGF signaling (Fig. 4). Notably, we identified many citrullinated structural proteins, such as myosin-10, myosin-9, microtubule-associated protein 4, filamin-A, filamin-C, fibronectin (FN1), tubulin alpha-1 C chain, and integrin beta-1 (Supplemental Table 2). The expression levels of some citrullinated peptides, including FN1 and transgelin (TAGLN), were significantly altered between biological conditions (Fig. 5). Citrullination of FN1 on arginine 1054 (R1054) was significantly upregulated in cells treated only with BB-Cl and cells pretreated with BB-Cl followed by TGF-β1 treatment (FC = 1.27 in the BB-Cl group and FC = 1.29 in the TGF-β1 + BB-Cl group in comparison to the control, $q < 0.05$) (Fig. 5A), which suggests that BB-CL amidine did not inhibit the activity of the PAD responsible for FN1citrullination. Interestingly, citrullination of TAGLN on arginine 12 (R12) was upregulated in TGF-β1-stimulated CFs (FC = 2.22 in the TGF-β1 group compared to the control group, $q = 0.08$) (Fig. 5B). In turn, citrullinated TLN1 on arginine 741 (R741) was not found in control CFs (Fig. 5C).

4. Discussion

Cardiac fibroblasts are the primary cell type responsible for fibrillar

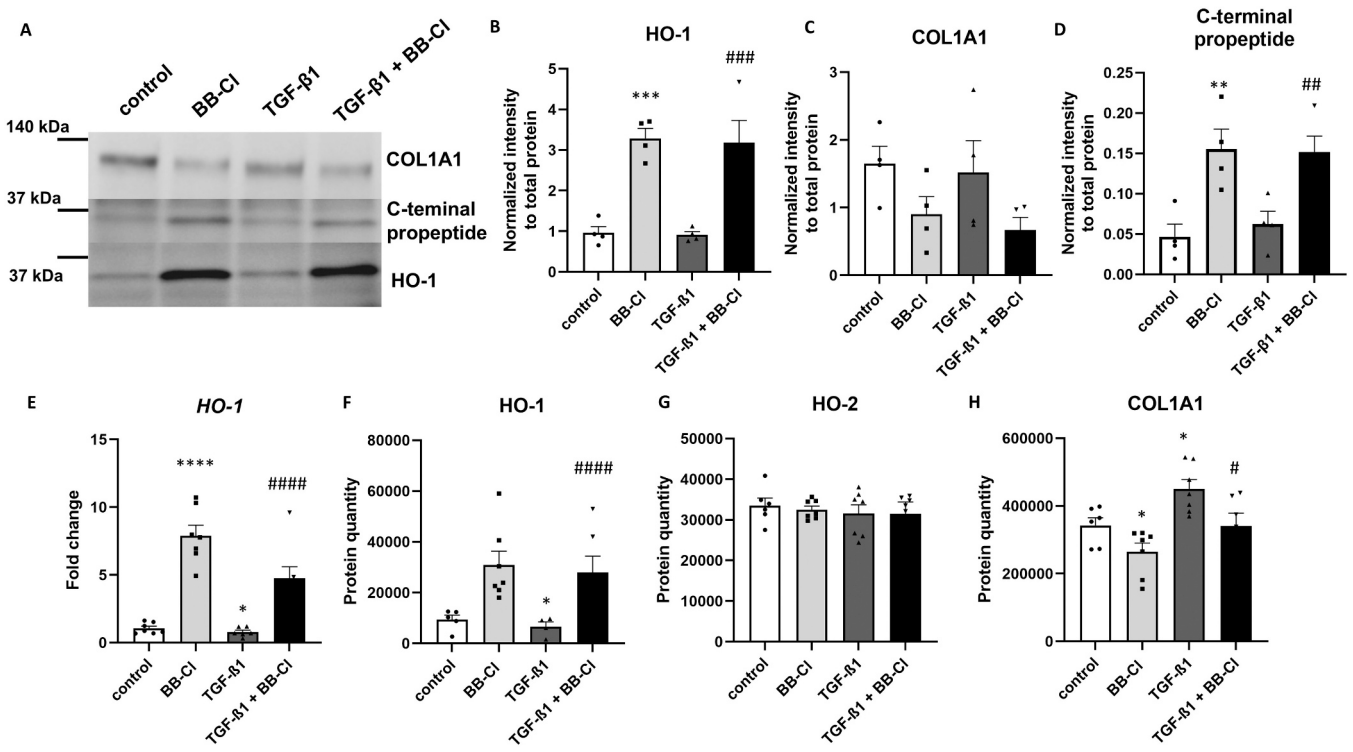

Fig. 3. BB-Cl administration led to the upregulation of heme oxygenase 1 (HO-1) in CFs and CFs differentiated into myoFbs. Western blot of COL1A1, COL1A1 C-terminal propeptide and HO-1 in CFs stimulated with TGF-β1 in the presence of BB-Cl A). Quantitative analysis of Western blots for HO-1 B), COL1A1 C) and COL1A1 C-terminal propeptide D) expression in CFs treated with TGF-β1 and BB-Cl. HO-1 mRNA expression in CFs treated with TGF-β1 and BB-Cl E). Protein quantities of HO-1 F), HO-2 G) and COL1A1 H) in CFs treated with TGF-β1 and BB-Cl as determined by proteomics. Mean ± SEM; *$p < 0.05$, **$p < 0.01$, ****$p < 0.0001$ compared to control; #$p < 0.05$, ##$p < 0.01$, ###$p < 0.001$, ####$p < 0.0001$compared to TGF-β1; n = 4 or 6–7.

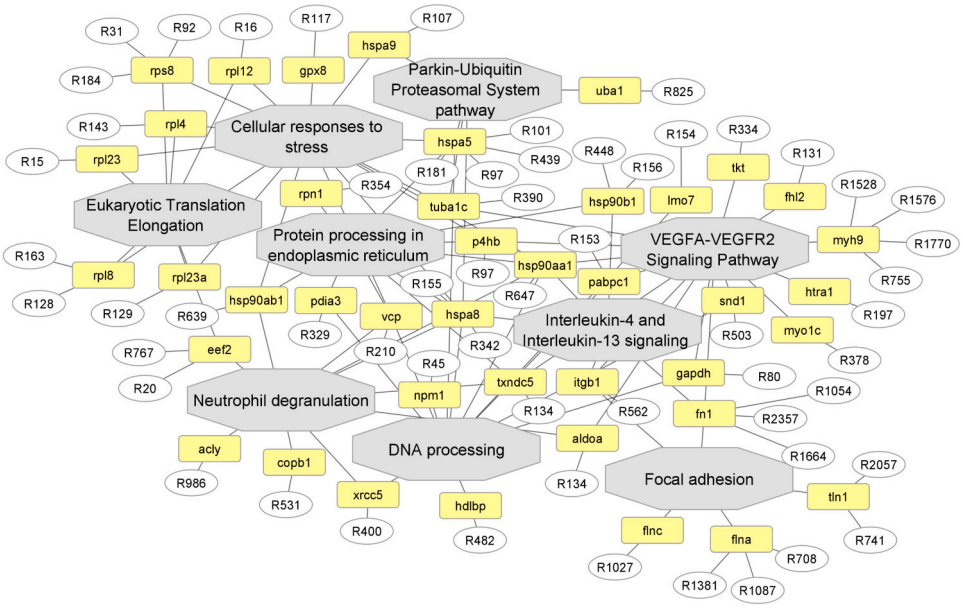

Fig. 4. Citrullination landscape of CFs differentiated into myoFbs. The identified and quantified citrullinated proteins were engaged in signaling by interleukins, neutrophil degranulation, focal adhesion, DNA processing and translation, proteasomal degradation, cellular response to stress, protein processing in the endoplasmic reticulum and VEGF signaling, among others.

collagen production and increased deposition in the myocardium under pathological conditions. As treatments are limited and regressing cardiac fibrosis represents a critical unmet need, an improved characterization of fibroblast phenotype changes is needed. In the present study, we demonstrated for the first time that 1) human CFs expressed PAD (PAD1 >PAD2 >PAD4, based on mRNA data), 2) 68 proteins were citrullinated across study groups, and 3) the pan-PAD inhibitor BB-Cl-amidine activated the Nrf2/HO-1 signaling pathway in CFs.

Our results indicated that CFs expressed PAD1, PAD2 and PAD4 transcripts, and PAD1 followed by PAD2 were the most abundant

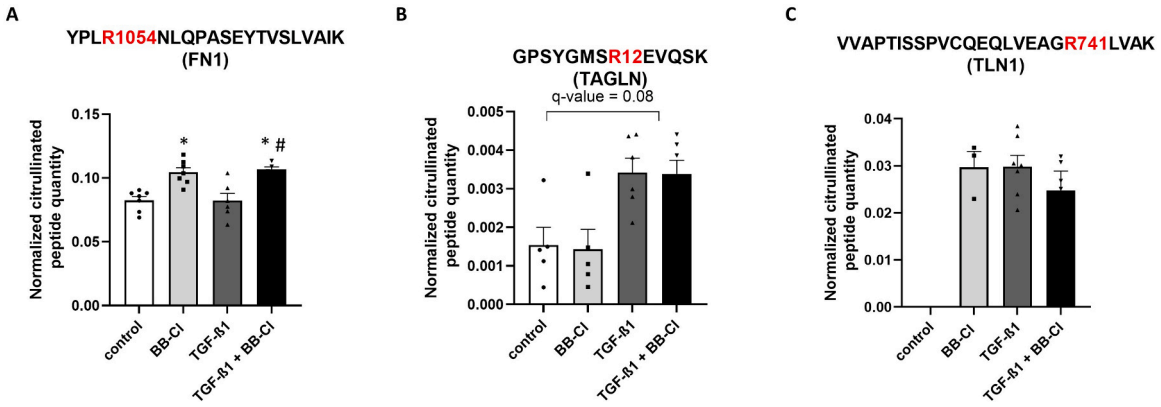

Fig. 5. Differentially enriched citrullinated peptides in CFs treated with TGF-β1 and BB-Cl. Normalized citrullinated peptide quantities of YPLR1054NLQPASEYTVSLVAIK (FN1) A), GPSYGMSR12EVQSK (TAGLN) B), and VVAPTISSPVCQEQLVEAGR741LVAK (TLN1) C) in CFs stimulated with TGF-β1 in the presence of BB-Cl. *q<0.05 compared to control, #q<0.05 compared to TGF-β1; n = 6–7.

isoforms, which is in line with data from mouse cardiomyocytes and mouse cardiac fibroblasts [31]. Importantly, we found that PAD1 was upregulated in TGF-β1-stimulated CFs, and BB-Cl administration led to the downregulation of PAD1 expression. Notably, BB-Cl-amidine inhibited TGF-β1 fibroblast activation, which was shown by the downregulation of PAD1 and PAD2 as well as the myofibroblast marker COL1A1.

Downregulation of COL1A1 upon BB-Cl-amidine administration was probably due to its degradation, as we observed upregulated COL1A1C-terminal propeptide in CFs and myoFbs treated with BB-Cl-amidine. Thus, BB-Cl treatment could lead to COL1A1 degradation and may have an impact on CF transdifferentiation to myoFbs.

In contrast, the mRNA expression levels of PAD4 did not increase after TGF-β1 stimulation for 24 h, but BB-Cl-amidine treatment upregulated its expression in TGF-β1-stimulated CFs. This finding could be an example of a compensatory mechanism by which CFs regulate PAD expression in response to BB-Cl-amidine treatment. Our results suggested that PAD1 and, to a lesser extent, PAD2 may influence/direct human CF transdifferentiation into myoFbs. Unfortunately, the low abundance of PADs and their untested stability in cell lysates may affect the proper interpretation of the data. Importantly, Akboua et al. pointed to the key role of PAD4 in the profibrotic phenotypes of murine cardiac fibroblasts. They showed that PAD4 was involved in the regulation of noncanonical TGF-β signaling, but knockout of PAD4 in CFs did not change fibrotic markers, except for collagen III [32]. In this paper, however, the authors used murine CFs, focused only on the role of PAD4, and did not assess expression levels of other PAD isoforms in murine CFs. Nevertheless, it is possible that PADs play an important role in the differentiation of CFs into myoFbs.

Notably, our proteomic analysis indicated upregulated expression of HO-1 in CFs differentiated into myoFbs. Importantly, BB-Cl administration led to an upregulation in HO-1 expression, which was confirmed by RT—qPCR and Western blot techniques. Furthermore, pathway analysis performed by IPA identified an enriched Nrf2-mediated oxidative stress response pathway and an activated Nrf2 transcription factor as an upstream regulator in myoFbs upon BB-Cl administration. Under normal conditions, Nrf2 remains sequestered in the cytoplasm by Keap1 (Kelch-like ECH-associated protein-1). However, when cells experience oxidative stress, Nrf2 is released from Keap-1 and translocates to the nucleus. Once in the nucleus, Nrf2 binds to the antioxidant response element (ARE) in the promoter regions of various genes, including the HO-1 gene. Nrf2 binding to the ARE enhances transcription of the HO-1 gene. The HO-1 enzyme catalyzes the degradation of heme, releasing biliverdin, carbon monoxide (CO) and iron, which act as potent antioxidant and anti-inflammatory molecules to induce cytoprotective effects against the damage caused by stress (ROS) and inflammation [33,34]. Recently, it has been shown that the Nfr2/HO-1 signaling pathway regulates cardiovascular homeostasis and can prevent cardiac remodeling and HF associated with oxidative stress [35,36]. Moreover, several studies have reported the upregulation of the Nrf2/HO-1 pathway and the inhibition of cardiac hypertrophy and fibrosis [37–40]. Similarly, upregulated HO-1 expression was related to the alleviation of oxidative stress and the inflammatory response in dermal fibroblasts [41]. However, it has also been shown that permanent activation of Nrf2 promotes pathological properties such as malignant cancer progression, chemo/radio resistance, and poor patient prognosis [42]. Interestingly, one study indicated the connection between citrullination and the Nrf2 signaling pathway. Citrulline treatment in LPS-induced acute lung injury led to the activation of the Nrf2 signaling pathway [43]. Overall, our results indicated that BB-Cl-amidine activated the Nrf2/HO-1 signaling pathway in CFs, which might have a protective effect against the transition of CFs to myoFbs. This might imply that PADs somehow regulate Nrf2 activity or its translocation to the nucleus, thus influencing the expression of HO-1 and other Nrf2-regulated genes. In CFs, activation of the Nrf2/HO-1 signaling pathway is crucial for protecting the cells from oxidative damage induced by various stressors, including reactive oxygen species (ROS) and inflammatory cytokines. Therefore, the pan-PAD inhibitor BB-Cl results in increased HO-1 expression via the Nrf2 pathway and may help CFs protect the heart from excessive tissue damage, thereby maintaining cardiac tissue integrity and function; however, further research is needed.

Furthermore, our MS data pointed to the downregulation of the SREBP pathway upon BB-Cl administration in activated CFs. Interestingly, SREBP1can activate profibrotic signaling by inducing TGFβ transcriptional activity and/or preventing exosomal degradation of the TGFβ receptor [44]. Thus, downregulation of the SREBP pathway might affect the activation of CFs to myoFbs upon BB-Cl treatment. Moreover, proteomic analyses revealed favorable changes in several proteins in response to BB-Cl-amidine administration in CFs activated to myoFbs. In particular, the expression of CSE was upregulated, whereas the expression of SULF1, Act A and RBM24 was downregulated in BB-Cl-treated, TGF-β1-stimulated CFs. CSE is one of the three enzymes that participates in the production of the endogenous gasotransmitter hydrogen sulfide (H_2S) in the cell. Importantly, it has been shown that exogenous H_2S treatment attenuates cardiac fibrosis through reactive oxygen species [45,46] and/or JAK/STAT signaling pathways [47]. Interestingly, administration of an exogenous H_2S donor prevented myocardial fibrosis by upregulating HO-1 and CSE expression [45]. Thus, upregulated expression of CSE upon BB-Cl administration may have beneficial effects in the treatment of cardiac fibrosis.

Moreover, we found downregulated expression of SULF1, Act A and

RBM24 in myoFbs treated with BB-Cl-amidine. Importantly, upregulated expression of these proteins was associated with the induction of cardiac fibrosis. SULF1 is a protein that is highly enriched in human and mouse myoFbs; its overexpression promotes myofibroblast activation, whereas its silencing attenuates myofibroblast activation and collagen deposition in vitro [48]. Act A is a potent activator of fibroblasts, belongs to the transforming growth factor-β superfamily and is involved in fibrosis and the inflammatory response [49]. Increased levels of Act A were reported to be associated with myocardial infarction, and its downregulated expression was related to the attenuation of cardiac fibrosis [50]. Notably, Act A upregulated COL1A1 mRNA expression in cultured cardiomyocytes and a rat model of HF [51]. Thus, the downregulated COL1A1 expression observed in our study in response to BB-Cl treatment in TGF-β1-stimulated CFs might be related to the downregulated expression of Act A; however, this notion requires further investigation. Moreover, RBM24 is a key splicing factor in the developing heart. Its overexpression has been shown to induce cardiac fibrosis by upregulating the expression of TGFβ signaling genes [52]. Whether downregulated expression of SULF1, Act A and RBM24 in BB-Cl-treated, TGF-β1-stimulated CFs is one of the favorable mechanisms of BB-Cl administration in cardiac fibrosis requires further study.

Importantly, we identified 86 citrullinated sites on 85 citrullinated peptides corresponding to 68 citrullinated proteins in CFs using a hypercitrullinated library approach combined with DIA-based LC—MS/MS. The quantified citrullinated proteins were involved in neutrophil degranulation, focal adhesion, DNA processing, translation elongation, proteasomal degradation, cellular response to stress, IL-4 and IL-13 signaling, protein processing in the endoplasmic reticulum and VEGF signaling. Moreover, we detected several citrullinated sites on structural proteins, such as myosin-10, myosin-9, microtubule-associated protein 4, filamin-A, filamin-C, FN1, tubulin alpha-1 C chain, and integrin beta-1 (Fig. 4). It has been reported that the citrullination of structural proteins has functional consequences on cell physiology. For example, citrullination of vimentin was shown to mediate the development and progression of lung fibrosis [53], whereas citrullination of collagen II was shown to affect integrin-mediated cell adhesion [54]. Moreover, citrullinated glial fibrillary acidic protein (GFAP) was implicated in the pathogenesis of hepatic fibrosis [55].

In our study, the expression level of citrullinated FN1 on arginine 1054 was increased in CFs and myoFbs treated with BB-Cl-amidine. This result might reflect the compensatory mechanism mediated by PAD4 upon pharmacological inhibition of PADs; however, further studies are necessary to validate this hypothesis. FN1 is a glycoprotein of the extracellular matrix that binds to integrins, collagen and fibrin, among others, and is primarily produced by CFs in the heart. FN1 polymerization promotes cell adhesion, growth, migration, and contractility and regulates the assembly of ECM proteins, such as collagen types I and III. FN1 levels are increased in ischemic cardiomyopathy and animal models of HF [56]. Moreover, FN1 is involved in the development of lung and liver fibrosis [57,58]. Inhibition of FN1 polymerization was shown to ameliorate adverse cardiac remodeling and fibrosis [59]. Interestingly, it has been reported that citrullinated FN1 plays a role in the pathogenesis of rheumatoid arthritis, where it alters the function of synovial fibroblasts [60]. It has been shown that citrullination of FN1 at R234 prevents integrin binding, thus potentially affecting extracellular matrix reassembly during joint inflammation [61]. Citrullination of FN1 was also found to alter integrin clustering and focal adhesion stability in fibroblasts [62]. In addition, citrullinated FN1 was shown to inhibit apoptosis and promote the secretion of proinflammatory cytokines in fibroblast-like synoviocytes [63]. However, the role of citrullinated FN1 in the pathogenesis of cardiac fibrosis has not been investigated and requires further study.

Furthermore, we found that citrullinated TAGLN on arginine 12 was upregulated in CFs differentiated into myoFbs by TGF-β1 stimulation. TAGLN, also named SM22α, is an actin-binding protein abundant in contractile vascular smooth muscle that plays an important role in the polymerization of sarcomeric actin filaments. It has been shown to be downregulated in atherosclerosis, abdominal aortic aneurysms and hypotension, and mice deficient in SM22α are prone to develop vascular diseases [64]. Interestingly, SM22α deletion has been reported to disrupt the architecture and function of caveolae and T-tubules in cardiomyocytes, contributing to HF [65]. Our results also indicated the lack of citrullinated TLN1 on arginine 741 in control CFs in comparison to BB-Cl- or TGF-β1-stimulated CFs. TLN1 is a cytoskeletal protein that links integrins to the actin cytoskeleton, thus mediating cell—cell adhesion. In the myocardium, it is a pivotal regulator of force transmission and transduction [66]. Loss of TLN1 and TLN2 in CFs has been reported to result in augmented ventricular cardiomyocyte hypertrophy in response to pressure overload [67]. In turn, the knockout of both TLN1 and TLN2 in cardiomyocytes led to cardiac dysfunction and HF [68]. However, the function of citrullinated TAGLN and TLN1 in CFs remains to be defined.

Our study has some limitations. We investigated the influence of a pan-PAD inhibitor, BB-Cl-amidine, on CF differentiation into myoFbs at the early stages of this process. However, we did not observe the prevention of CF transdifferentiation to myoFbs by the pan-PAD inhibitor BB-Cl-amidine; thus, it would be interesting to perform similar experiments including advanced stages of CF transdifferentiation to myoFbs. Furthermore, we cultured the CFs on gelatin-coated dishes that enable humanized culture conditions, which cannot be directly compared to studies on regular tissue culture plastic plates. Studies on regular tissue culture plates have shown enhanced endogenous TGF-β release from the extracellular matrix, which primes the TGF-β pathway to promote fibroblast differentiation [69–71]. Finally, we used commercially available CFs that were isolated from normal human fetal hearts. It is worth noting that CFs isolated from the hearts of older and diseased donors could exhibit different patterns of PAD expression.

Overall, our results indicated the activation of the Nrf2/HO-1 signaling pathway in CFs upon BB-Cl administration (Fig. 6). However, the functional roles of PADs and the identified novel citrullinated sites in CFs and their involvement in the regulation of cardiac fibrosis require further study.

5. Conclusions

Our findings demonstrate that PAD1 expression was upregulated during CF transdifferentiation into myoFbs and that the pan-PAD inhibitor BB-Cl-amidine downregulated both PAD1 and PAD2 expression in both CFs and myoFbs. This effect was related to the upregulation of HO-1 expression and the downregulation of the fibrosis marker COL1A1 due to its degradation. Moreover, MS analyses indicated that the Nrf2/HO-1 signaling pathway was activated in CFs upon BB-Cl administration. These results suggested that inhibiting PAD in CFs could be a novel therapeutic strategy in the treatment of cardiac fibrosis. Importantly, we identified 86 citrullination sites in CFs, and the majority of the citrullinated proteins belonged to signaling pathways mediating focal adhesion, inflammation, and DNA processing, the key cellular mediators of fibrosis. We hope that knowledge concerning the changes in citrullinated proteins during the fibrotic process can provide new insights for subsequent in-depth fibrosis research and facilitate the advancement of therapeutic targets that regulate myoFb activation, extracellular matrix cross-linking, metabolism, and inflammation in fibrosis.

Funding

This research was supported by the Polish National Agency for Academic Exchange (NAWA).

CRediT authorship contribution statement

Aneta Stachowicz: Conceptualization, Methodology, Formal analysis, Investigation, Writing – original draft, Visualization. **Brian**

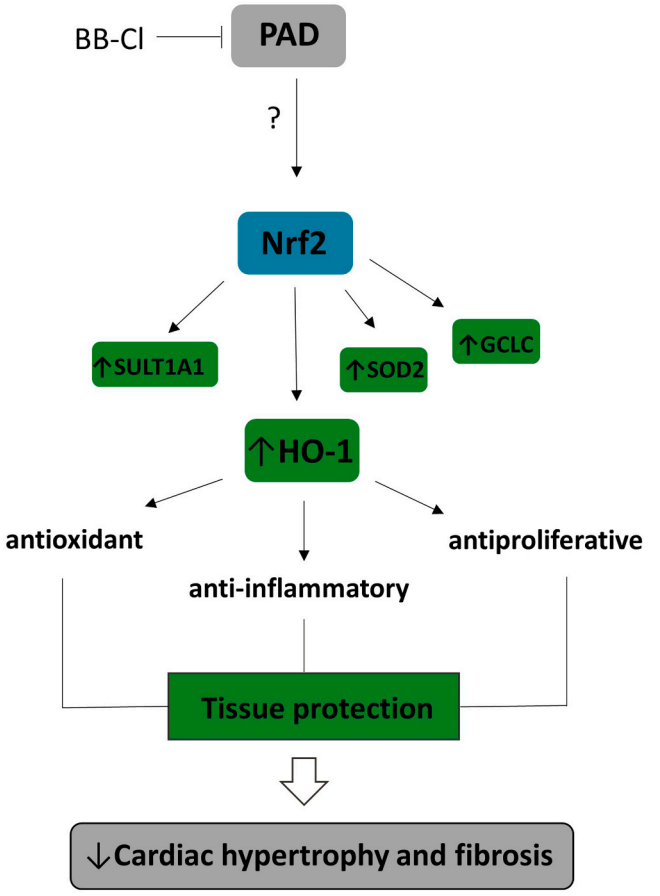

Fig. 6. BB-Cl administration activates the Nrf2/HO-1 signaling pathway in human cardiac fibroblasts. BB-Cl treatment leads to the upregulation of HO-1 and other cytoprotective genes (SOD2, GCLC, SULT1A1). HO-1 provides tissue protection through antioxidant, anti-inflammatory and antiproliferative effects, which could inhibit cardiac hypertrophy and fibrosis.

Walker: Investigation. **Alia Sadiq:** Formal analysis, Visualization. **Niveda Sundararaman:** Formal analysis, Software. **Justyna Fert-Bober:** Conceptualization, Methodology, Investigation, Formal analysis, Writing – review & editing, Supervision.

Declaration of Competing Interest

The authors declare no conflicts of interest.

Acknowledgments

AS, JFB were responsible for the conception and design of the study. AS, BW, NS were responsible for analyses of the samples. AS, AS, JFB were responsible for the interpretation of the data. AS and JFB drafted the article. All authors critically revised the paper for important intellectual content and gave final approval of the version to be published.

Appendix A. Supporting information

Supplementary data associated with this article can be found in the online version at doi:10.1016/j.biopha.2023.115443.

References

[1] M. Sweeney, B. Corden, S.A. Cook, Targeting cardiac fibrosis in heart failure with preserved ejection fraction: mirage or miracle? EMBO Mol. Med. 12 (2020), e10865 https://doi.org/10.15252/emmm.201910865.

[2] G. Savarese, L.H. Lund, Global public health burden of heart failure, Card. Fail. Rev. 3 (2017) 7–11, https://doi.org/10.15420/cfr.2016:25:2.

[3] J. Fert-Bober, J. Sokolove, Proteomics of citrullination in cardiovascular disease, Proteom. Clin. Appl. 8 (2014) 522–533, https://doi.org/10.1002/prca.201400013.

[4] N. Kittana, Angiotensin-converting enzyme 2-Angiotensin 1-7/1-9 system: novel promising targets for heart failure treatment, Fundam. Clin. Pharmacol. 32 (2018) 14–25, https://doi.org/10.1111/fcp.12318.

[5] W. Jiang, Y. Xiong, X. Li, Y. Yang, Cardiac fibrosis: cellular effectors, molecular pathways, and exosomal roles, Front. Cardiovasc. Med. 8 (2021). ⟨https://www.frontiersin.org/articles/10.3389/fcvm.2021.715258⟩ (accessed March 23, 2023).

[6] P. Kong, P. Christia, N.G. Frangogiannis, The pathogenesis of cardiac fibrosis, Cell. Mol. Life Sci. 71 (2014) 549–574, https://doi.org/10.1007/s00018-013-1349-6.

[7] H. Kurose, Cardiac fibrosis and fibroblasts, Cells 10 (2021) 1716, https://doi.org/10.3390/cells10071716.

[8] K. Yan, K. Wang, P. Li, The role of posttranslational modifications in cardiac hypertrophy, J. Cell. Mol. Med. 23 (2019) 3795–3807, https://doi.org/10.1111/jcmm.14330.

[9] B. György, E. Tóth, E. Tarcsa, A. Falus, E.I. Buzás, Citrullination: a posttranslational modification in health and disease, Int. J. Biochem. Cell Biol. 38 (2006) 1662–1677, https://doi.org/10.1016/j.biocel.2006.03.008.

[10] E.E. Witalison, P.R. Thompson, L.J. Hofseth, Protein arginine deiminases and associated citrullination: physiological functions and diseases associated with dysregulation, Curr. Drug Targets 16 (2015) 700–710.

[11] J.L. Slack, C.P. Causey, P.R. Thompson, Protein arginine deiminase 4: a target for an epigenetic cancer therapy, Cell. Mol. Life Sci. 68 (2011) 709–720, https://doi.org/10.1007/s00018-010-0480-x.

[12] M.A. Christophorou, G. Castelo-Branco, R.P. Halley-Stott, C.S. Oliveira, R. Loos, A. Radzisheuskaya, K.A. Mowen, P. Bertone, J.C.R. Silva, M. Zernicka-Goetz, M. L. Nielsen, J.B. Gurdon, T. Kouzarides, Citrullination regulates pluripotency and histone H1 binding to chromatin, Nature 507 (2014) 104–108, https://doi.org/10.1038/nature12942.

[13] J. Kawalkowska, A.-M. Quirke, F. Ghari, S. Davis, V. Subramanian, P.R. Thompson, R.O. Williams, R. Fischer, N.B. La Thangue, P.J. Venables, Abrogation of collagen-induced arthritis by a peptidyl arginine deiminase inhibitor is associated with modulation of T-cell-mediated immune responses, Sci. Rep. 6 (2016) 26430, https://doi.org/10.1038/srep26430.

[14] M. Beato, P. Sharma, Peptidyl arginine deiminase 2 (PADI2)-mediated arginine citrullination modulates transcription in cancer, Int. J. Mol. Sci. 21 (2020) 1351, https://doi.org/10.3390/ijms21041351.

[15] L. Wang, H. Chen, J. Tang, Z. Guo, Y. Wang, Peptidylarginine deiminase and Alzheimer's disease, J. Alzheimers Dis. 85 (2022) 473–484, https://doi.org/10.3233/JAD-215302.

[16] D. Zhu, Y. Lu, Y. Wang, Y. Wang, PAD4 and its inhibitors in cancer progression and prognosis, Pharmaceutics 14 (2022) 2414, https://doi.org/10.3390/pharmaceutics14112414.

[17] M. Du, W. Yang, S. Schmull, J. Gu, S. Xue, Inhibition of peptidyl arginine deiminase-4 protects against myocardial infarction induced cardiac dysfunction, Int. Immunopharmacol. 78 (2020), 106055, https://doi.org/10.1016/j.intimp.2019.106055.

[18] K. Eghbalzadeh, L. Georgi, T. Louis, H. Zhao, U. Keser, C. Weber, M. Mollenhauer, A. Conforti, T. Wahlers, A. Paunel-Görgülü, Compromised anti-inflammatory action of neutrophil extracellular traps in PAD4-deficient mice contributes to aggravated acute inflammation after myocardial infarction, Front. Immunol. 10 (2019). ⟨https://www.frontiersin.org/articles/10.3389/fimmu.2019.02313⟩ (accessed March 14, 2023).

[19] K. Martinod, T. Witsch, L. Erpenbeck, A. Savchenko, H. Hayashi, D. Cherpokova, M. Gallant, M. Mauler, S.M. Cifuni, D.D. Wagner, Peptidylarginine deiminase 4 promotes age-related organ fibrosis, J. Exp. Med. 214 (2017) 439–458, https://doi.org/10.1084/jem.20160530.

[20] A. Stachowicz, R. Olszanecki, M. Suski, A. Wiśniewska, J. Totoń-Żurańska, J. Madej, J. Jawień, M. Białas, K. Okoń, M. Gajda, K. Głombik, A. Basta-Kaim, R. Korbut, Mitochondrial aldehyde dehydrogenase activation by alda-1 inhibits atherosclerosis and attenuates hepatic steatosis in apolipoprotein e-knockout mice, J. Am. Heart Assoc. 3 (2014), https://doi.org/10.1161/JAHA.114.001329.

[21] J.R. Wiśniewski, A. Zougman, M. Mann, Combination of FASP and StageTip-based fractionation allows in-depth analysis of the hippocampal membrane proteome, J. Proteome Res. 8 (2009) 5674–5678, https://doi.org/10.1021/pr900748n.

[22] J.R. Wiśniewski, D. Rakus, Multienzyme digestion FASP and the 'Total Protein Approach'-based absolute quantification of the Escherichia coli proteome, J. Proteom. 109 (2014) 322–331, https://doi.org/10.1016/j.jprot.2014.07.012.

[23] A. Stachowicz, N. Sundararaman, V. Venkatraman, J. Van Eyk, J. Fert-Bober, pH/acetonitrile-gradient reversed-phase fractionation of enriched hyper-citrullinated library in combination with LC–MS/MS analysis for confident identification of citrullinated peptides, Methods Mol. Biol. 2420 (2022) 107–126, https://doi.org/10.1007/978-1-0716-1936-0_9.

[24] R. Bruderer, O.M. Bernhardt, T. Gandhi, S.M. Miladinović, L.-Y. Cheng, S. Messner, T. Ehrenberger, V. Zanotelli, Y. Butscheid, C. Escher, O. Vitek, O. Rinner, L. Reiter, Extending the limits of quantitative proteome profiling with data-independent acquisition and application to acetaminophen-treated three-dimensional liver microtissues, Mol. Cell. Proteom. 14 (2015) 1400–1410, https://doi.org/10.1074/mcp.M114.044305.

[25] T. Huang, R. Bruderer, J. Muntel, Y. Xuan, O. Vitek, L. Reiter, Combining precursor and fragment information for improved detection of differential abundance in data independent acquisition, Mol. Cell. Proteom. 19 (2020) 421–430, https://doi.org/10.1074/mcp.RA119.001705.

[26] J.D. Story, A direct approach to false discovery rates, J. R. Stat. Soc. Ser. B Stat. Methodol. 64 (2002) 479–498, https://doi.org/10.1111/1467-9868.00346.
[27] J. Fert-Bober, V. Venkatraman, C.L. Hunter, R. Liu, E.L. Crowgey, R. Pandey, R. J. Holewinski, A. Stotland, B.P. Berman, J.E. Van Eyk, Mapping citrullinated sites in multiple organs of mice using hypercitrullinated library, J. Proteome Res. 18 (2019) 2270–2278, https://doi.org/10.1021/acs.jproteome.9b00118.
[28] S. Tyanova, T. Temu, P. Sinitcyn, A. Carlson, M.Y. Hein, T. Geiger, M. Mann, J. Cox, The Perseus computational platform for comprehensive analysis of (prote) omics data, Nat. Methods 13 (2016) 731–740, https://doi.org/10.1038/nmeth.3901.
[29] N. Sundararaman, J. Go, A.E. Robinson, J.M. Mato, S.C. Lu, J.E. Van Eyk, V. Venkatraman, PINE: an automation tool to extract and visualize protein-centric functional networks, J. Am. Soc. Mass Spectrom. 31 (2020) 1410–1421, https://doi.org/10.1021/jasms.0c00032.
[30] J.A. Vizcaíno, E.W. Deutsch, R. Wang, A. Csordas, F. Reisinger, D. Ríos, J. A. Dianes, Z. Sun, T. Farrah, N. Bandeira, P.-A. Binz, I. Xenarios, M. Eisenacher, G. Mayer, L. Gatto, A. Campos, R.J. Chalkley, H.-J. Kraus, J.P. Albar, S. Martinez-Bartolomé, R. Apweiler, G.S. Omenn, L. Martens, A.R. Jones, H. Hermjakob, ProteomeXchange provides globally coordinated proteomics data submission and dissemination, Nat. Biotechnol. 32 (2014) 223–226, https://doi.org/10.1038/nbt.2839.
[31] J. Fert-Bober, J.T. Giles, R.J. Holewinski, J.A. Kirk, H. Uhrigshardt, E.L. Crowgey, F. Andrade, C.O. Bingham, J.K. Park, M.K. Halushka, D.A. Kass, J.M. Bathon, J. E. Van Eyk, Citrullination of myofilament proteins in heart failure, Cardiovasc. Res. 108 (2015) 232–242, https://doi.org/10.1093/cvr/cvv185.
[32] H. Akboua, K. Eghbalzadeh, U. Keser, T. Wahlers, A. Paunel-Görgülü, Impaired noncanonical transforming growth factor-β signaling prevents profibrotic phenotypes in cultured peptidylarginine deiminase 4-deficient murine cardiac fibroblasts, J. Cell. Mol. Med. 25 (2021) 9674–9684, https://doi.org/10.1111/jcmm.16915.
[33] S.W. Ryter, Heme oxygenase-1: an anti-inflammatory effector in cardiovascular, lung, and related metabolic disorders, Antioxidants 11 (2022) 555, https://doi.org/10.3390/antiox11030555.
[34] F. He, X. Ru, T. Wen, NRF2, a transcription factor for stress response and beyond, Int. J. Mol. Sci. 21 (2020) 4777, https://doi.org/10.3390/ijms21134777.
[35] X. Zhang, Y. Yu, H. Lei, Y. Cai, J. Shen, P. Zhu, Q. He, M. Zhao, The Nrf-2/HO-1 signaling axis: a ray of hope in cardiovascular diseases, Cardiol. Res. Pract. 2020 (2020), e5695723, https://doi.org/10.1155/2020/5695723.
[36] S. Zhou, W. Sun, Z. Zhang, Y. Zheng, The role of Nrf2-mediated pathway in cardiac remodeling and heart failure, Oxid. Med. Cell. Longev. 2014 (2014), 260429, https://doi.org/10.1155/2014/260429.
[37] X. Liu, A.S. Pachori, C.A. Ward, J.P. Davis, M. Gnecchi, D. Kong, L. Zhang, J. Murduck, S.-F. However, M.A. Perrella, R.E. Pratt, V.J. Dzau, L.G. Melo, Heme oxygenase-1 (HO-1) inhibits postmyocardial infarct remodeling and restores ventricular function, FASEB J. Off. Publ. Fed. Am. Soc. Exp. Biol. 20 (2006) 207–216, https://doi.org/10.1096/fj.05-4435com.
[38] C. Tang, G. Yin, C. Huang, H. Wang, J. Gao, J. Luo, Z. Zhang, J. Wang, J. Hong, X. Chai, Peroxiredoxin-1 ameliorates pressure overload-induced cardiac hypertrophy and fibrosis, Biomed. Pharmacother. 129 (2020), 110357, https://doi.org/10.1016/j.biopha.2020.110357.
[39] Y. Li, J.-Z. Duan, Q. He, C.-Q. Wang, miR-155 modulates high glucose-induced cardiac fibrosis via the Nrf2/HO-1 signaling pathway, Mol. Med. Rep. 22 (2020) 4003–4016, https://doi.org/10.3892/mmr.2020.11495.
[40] Z. Meng, H.-Y. Li, C.-Y. Si, Y.-Z. Liu, S. Teng, Asiatic acid inhibits cardiac fibrosis throughNrf2/HO-1 and TGF-β1/Smads signaling pathways in spontaneous hypertension rats, Int. Immunopharmacol. 74 (2019), 105712, https://doi.org/10.1016/j.intimp.2019.105712.
[41] Q. Li, S. Liang, Q. Lai, L. Shen, Y. Zhang, R. Guo, Heme oxygenase-1 alleviates advanced glycation end product-induced oxidative stress, inflammatory response and biological behavioral disorders in rat dermal fibroblasts, Exp. Ther. Med. 22 (2021) 1212, https://doi.org/10.3892/etm.2021.10646.
[42] F. Pouremamali, A. Pouremamali, M. Dadashpour, N. Soozangar, F. Jeddi, An update of Nrf2 activators and inhibitors in cancer prevention/promotion, Cell Commun. Signal. 20 (2022) 100, https://doi.org/10.1186/s12964-022-00906-3.
[43] Y. Xue, Y. Zhang, L. Chen, Y. Wang, Z. Lv, L.-Q. Yang, S. Li, Citrulline protects against LPS-induced acute lung injury by inhibiting ROS/NLRP3–dependent pyroptosis and apoptosis via the Nrf2 signaling pathway, Exp. Ther. Med. 24 (2022) 632, https://doi.org/10.3892/etm.2022.11569.
[44] D. Dorotea, D. Koya, H. Ha, Recent insights into SREBP as a direct mediator of kidney fibrosis via lipid-independent pathways, Front. Pharmacol. 11 (2020) 265, https://doi.org/10.3389/fphar.2020.00265.
[45] L.-L. Pan, X.-H. Liu, Y.-Q. Shen, N.-Z. Wang, J. Xu, D. Wu, Q.-H. Xiong, H.-Y. Deng, G.-Y. Huang, Y.-Z. Zhu, Inhibition of NADPH oxidase 4-related signaling by sodium hydrosulfide attenuates myocardial fibrotic response, Int. J. Cardiol. 168 (2013) 3770–3778, https://doi.org/10.1016/j.ijcard.2013.06.007.
[46] D. Zheng, S. Dong, T. Li, F. Yang, X. Yu, J. Wu, X. Zhong, Y. Zhao, L. Wang, C. Xu, F. Lu, W. Zhang, Exogenous hydrogen sulfide attenuates cardiac fibrosis through reactive oxygen species signal pathways in experimental diabetes mellitus models, Cell. Physiol. Biochem. Int. J. Exp. Cell. Physiol. Biochem. Pharmacol. 36 (2015) 917–929, https://doi.org/10.1159/000430266.
[47] M. Liu, Y. Li, B. Liang, Z. Li, Z. Jiang, C. Chu, J. Yang, Hydrogen sulfide attenuates myocardial fibrosis in diabetic rats through the JAK/STAT signaling pathway, Int. J. Mol. Med. 41 (2018) 1867–1876, https://doi.org/10.3892/ijmm.2018.3419.
[48] J. Wu, K.C.V. Subbaiah, L.H. Xie, F. Jiang, E.-S. Khor, D. Mickelsen, J.R. Myers, W. H.W. Tang, P. Yao, Glutamyl-prolyl-tRNA synthetase regulates proline-rich pro-fibrotic protein synthesis during cardiac fibrosis, Circ. Res. 127 (2020) 827–846, https://doi.org/10.1161/CIRCRESAHA.119.315999.
[49] S. Yamashita, A. Maeshima, I. Kojima, Y. Nojima, Activin A is a potent activator of renal interstitial fibroblasts, J. Am. Soc. Nephrol. 15 (2004) 91–101, https://doi.org/10.1097/01.asn.0000103225.68136.e6.
[50] C. Yang, J. Liu, K. Liu, B. Du, K. Shi, M. Ding, B. Li, P. Yang, Ghrelin suppresses cardiac fibrosis of postmyocardial infarction heart failure rats by adjusting the activin A-follistatin imbalance, Peptides 99 (2018) 27–35, https://doi.org/10.1016/j.peptides.2017.10.018.
[51] Q. Wei, Y.-N. Wang, H.-Y. Liu, J. Yang, C.-Y. Yang, M. Liu, Y.-F. Liu, P. Yang, Z.-H. Liu, The expression and role of activin A and follistatin in heart failure rats after myocardial infarction, Int. J. Cardiol. 168 (2013) 2994–2997, https://doi.org/10.1016/j.ijcard.2013.04.012.
[52] M.M.G. van den Hoogenhof, I. van der Made, N.E. de Groot, A. Damanafshan, S.C. M. van Amersfoorth, L. Zentilin, M. Giacca, Y.M. Pinto, E.E. Creemers, AAV9-mediated Rbm24 overexpression induces fibrosis in the mouse heart, Sci. Rep. 8 (2018), 11696, https://doi.org/10.1038/s41598-018-29552-x.
[53] F.J. Li, R. Surolia, H. Li, Z. Wang, G. Liu, T. Kulkarni, A.V.F. Massicano, J. A. Mobley, S. Mondal, J.A. de Andrade, S.A. Coonrod, P.R. Thompson, K. Wille, S. E. Lapi, M. Athar, V.J. Thannickal, A.B. Carter, V.B. Antony, Citrullinated vimentin mediates development and progression of lung fibrosis, Sci. Transl. Med. 13 (2021) eaba2927, https://doi.org/10.1126/scitranslmed.aba2927.
[54] K. Sipilä, S. Haag, K. Denessiouk, J. Käpylä, E.C. Peters, A. Denesyuk, U. Hansen, Y. Konttinen, M.S. Johnson, R. Holmdahl, J. Heino, Citrullination of collagen II affects integrin-mediated cell adhesion in a receptor-specific manner, FASEB J. Off. Publ. Fed. Am. Soc. Exp. Biol. 28 (2014) 3758–3768, https://doi.org/10.1096/fj.13-247767.
[55] S.-E. Kim, J.W. Park, M.-J. Kim, B. Jang, Y.-C. Jeon, H.-J. Kim, A. Ishigami, H. S. Kim, K.T. Suk, D.J. Kim, C.K. Park, E.-K. Choi, M.-K. Jang, Accumulation of citrullinated glial fibrillary acidic protein in a mouse model of bile duct ligation-induced hepatic fibrosis, PLoS One 13 (2018), e0201744, https://doi.org/10.1371/journal.pone.0201744.
[56] A. Heling, R. Zimmermann, S. Kostin, Y. Maeno, S. Hein, B. Devaux, E. Bauer, W.-P. Klövekorn, M. Schlepper, W. Schaper, J. Schaper, Increased expression of cytoskeletal, linkage, and extracellular proteins in failing human myocardium, Circ. Res. 86 (2000) 846–853, https://doi.org/10.1161/01.RES.86.8.846.
[57] A.F. Muro, F.A. Moretti, B.B. Moore, M. Yan, R.G. Atrasz, C.A. Wilke, K.R. Flaherty, F.J. Martinez, J.L. Tsui, D. Sheppard, F.E. Baralle, G.B. Toews, E.S. White, An essential role for fibronectin extra type III domain An in pulmonary fibrosis, Am. J. Respir. Crit. Care Med. 177 (2008) 638–645, https://doi.org/10.1164/rccm.200708–1291 °C.
[58] W.R. Jarnagin, D.C. Rockey, V.E. Koteliansky, S.S. Wang, D.M. Bissell, Expression of variant fibronectins in wound healing: cellular source and biological activity of the EIIIA segment in rat hepatic fibrogenesis, J. Cell Biol. 127 (1994) 2037–2048, https://doi.org/10.1083/jcb.127.6.2037.
[59] I. Valiente-Alandi, S.J. Potter, A.M. Salvador, A.E. Schafer, T. Schips, F. Carrillo-Salinas, A.M. Gibson, M.L. Nieman, C. Perkins, M.A. Sargent, J. Huo, J.N. Lorenz, T. DeFalco, J.D. Molkentin, P. Alcaide, B.C. Blaxall, Inhibiting fibronectin attenuates fibrosis and improves cardiac function in a model of heart failure, Circulation 138 (2018) 1236–1252, https://doi.org/10.1161/CIRCULATIONAHA.118.034609.
[60] M.A. Shelef, D.A. Bennin, D.F. Mosher, A. Huttenlocher, Citrullination of fibronectin modulates synovial fibroblast behavior, Arthritis Res. Ther. 14 (2012) R240, https://doi.org/10.1186/ar4083.
[61] K.H. Sipilä, V. Ranga, P. Rappu, M. Mali, L. Pirilä, I. Heino, J. Jokinen, J. Käpylä, M.S. Johnson, J. Heino, Joint inflammation related citrullination of functional arginines in extracellular proteins, Sci. Rep. 7 (2017) 8246, https://doi.org/10.1038/s41598-017-08597-4.
[62] V.L. Stefanelli, S. Choudhury, P. Hu, Y. Liu, A. Schwenzer, C.-R. Yeh, D. M. Chambers, K. von Beck, W. Li, T. Segura, K.S. Midwood, M. Torres, T.H. Barker, Citrullination of fibronectin alters integrin clustering and focal adhesion stability promoting stromal cell invasion, Matrix Biol. J. Int. Soc. Matrix Biol. 82 (2019) 86–104, https://doi.org/10.1016/j.matbio.2019.04.002.
[63] L. Fan, Q. Wang, R. Liu, M. Zong, D. He, H. Zhang, Y. Ding, J. Ma, Citrullinated fibronectin inhibits apoptosis and promotes the secretion of pro-inflammatory cytokines in fibroblast-like synoviocytes in rheumatoid arthritis, Arthritis Res. Ther. 14 (2012) R266, https://doi.org/10.1186/ar4112.
[64] R. Chen, F. Zhang, L. Song, Y. Shu, Y. Lin, L. Dong, X. Nie, D. Zhang, P. Chen, M. Han, Transcriptome profiling reveals that the SM22α-regulated molecular pathways contribute to vascular pathology, J. Mol. Cell. Cardiol. 72 (2014) 263–272, https://doi.org/10.1016/j.yjmcc.2014.04.003.
[65] J. Wu, W. Wang, Y. Huang, H. Wu, J. Wang, M. Han, Deletion of SM22α disrupts the structure and function of caveolae and T-tubules in cardiomyocytes, contributing to heart failure, PLoS ONE 17 (2022), e0271578, https://doi.org/10.1371/journal.pone.0271578.
[66] K. Austen, P. Ringer, A. Mehlich, A. Chrostek-Grashoff, C. Kluger, C. Klingner, B. Sabass, R. Zent, M. Rief, C. Grashoff, Extracellular rigidity sensing by talin isoform-specific mechanical linkages, Nat. Cell Biol. 17 (2015) 1597–1606, https://doi.org/10.1038/ncb3268.
[67] N.A. Noll, L.A. Riley, C.S. Moore, L. Zhong, M.R. Bersi, J.D. West, R. Zent, W. D. Merryman, Loss of talin in cardiac fibroblasts results in augmented ventricular cardiomyocyte hypertrophy in response to pressure overload, Am. J. Physiol. Heart Circ. Physiol. 322 (2022) H857–H866, https://doi.org/10.1152/ajpheart.00632.2021.
[68] A.M. Manso, H. Okada, F.M. Sakamoto, E. Moreno, S.J. Monkley, R. Li, D. R. Critchley, R.S. Ross, Loss of mouse cardiomyocyte talin-1 and talin-2 leads to β-1

integrin reduction, costameric instability, and dilated cardiomyopathy, Proc. Natl. Acad. Sci. 114 (2017) E6250–E6259, https://doi.org/10.1073/pnas.1701416114.
[69] T. Meyer-ter-Vehn, H. Han, F. Grehn, G. Schlunck, Extracellular matrix elasticity modulates TGF-β–induced p38 activation and myofibroblast transdifferentiation in human tenon fibroblasts, Investig. Ophthalmol. Vis. Sci. 52 (2011) 9149–9155, https://doi.org/10.1167/iovs.10-6679.
[70] J.L. Allen, M.E. Cooke, T. Alliston, ECM stiffness primes the TGFβ pathway to promote chondrocyte differentiation, Mol. Biol. Cell 23 (2012) 3731–3742, https://doi.org/10.1091/mbc.E12-03-0172.
[71] Q. Xu, J.T. Norman, S. Shrivastav, J. Lucio-Cazana, J.B. Kopp, *In vitro* models of TGF-β-induced fibrosis suitable for high-throughput screening of antifibrotic agents, Am. J. Physiol. Ren. Physiol. 293 (2007) F631–F640, https://doi.org/10.1152/ajprenal.00379.2006.